Supplementary data B

B1. **Microbial community profile analysis**

Genomic DNA of the total microbial community was extracted on cells pelleted from 5 mL supernatant using the MOBIO PowerSoil DNA Isolation Kit (MOBio, Carlsbad Springs, USA), following the manufacturer protocol, with an additional 10 min initial heating period at 55°C. Sample DNA was quantified using a Take3 spectrophotometry system on a Synergy HI microplate reader (BioTek, Winooski VT, USA). Sequencing of DNA samples was carried out on an Illumina MiSeq system (Illumina Biotechnology Co., San Diego, USA) by Metagenom Bio Inc. (Toronto, Canada), targeting the bacterial 16S rRNA genes using primers Pro341F (5'-CCT ACG GGN BGC ASC AG-3') and Pro805R (5'-GAC TAC NVG GGT ATC TAA TCC-3) (Takahashi et al., 2014). A 25 µL PCR (polymerase chain reaction) was performed containing 5 µl of standard OneTaq buffer 5 x 0.25 µL of 25 mM dNTP (deoxyribose nucleoside triphosphate) containing, 0.5 µL of both the forward and reverse primers, 1 µL BSA (bovine serum albumin, 12 mg mL^{-1}), 0.125 µL of OneTaq DNA polymerase (New England Bio, MA, USA), 1-10 ng DNA and water to equal a total reaction volume of 25 µL. Initial denaturation started at 94 °C for 5 mins followed by 30 cycles of 94 °C for 30 sec denaturation, annealing was at 53 °C for 16 s, for 45 sec, extension at 68 °C for 1 min with a final extension step at 68 °C for 10 minutes. PCRs were done in triplicate for each sample to reduce PCR bias and products were checked on a 2% agarose gel, after which the bands were excised with a MinElute gel extraction kit (Qiagen, Hilden, Germany). The purified DNA libraries were quantified on a Quibit with the dsDNA HS assay kit (Life Technologies, CA, USA), the library pools were spiked with 5% phix control (V3, Illumina) to improve base imbalance, and paired-end sequencing with read lengths of 250 bp was performed using MiSeq Reagent kit V2 (2 x 250 cycles) on a Illumina MiSeq platform. Raw Miseq reads were merged using PANDAseq for the 16S rRNA gene reads. All reads were then further quality filtered using USEARCH v8.1.1861, and taxonomy was assigned using QIIME with the Green Genes database. Data were then imported and analyzed with the R software using the phyloseq package.

The Cr $2p_{3/2}$ spectrum of an untreated chromitite

The Cr 2p spectra is composed of the Cr $2p_{1/2}$ and Cr $2p_{3/2}$ envelopes which are 10 eV apart (Figure B1a). Both Cr 2p envelopes store the same information about the speciation and valence of Cr. In the Cr $2p_{3/2}$ envelope, bands for Cr^{3+} and Cr^{6+} components occur at circa 577-578 eV and 579-580 eV, respectively (Biesinger et al. 2004, 2011). Satellite peaks for Cr^{3+} compounds may be visible in the spectrum at 597 eV for the Cr $2p_{1/2}$ spectrum and at 587 eV for the Cr $2p_{3/2}$ spectrum (the latter being overlapped by the Cr $2p_{1/2}$ spectrum). The shift to higher binding energy with increasing valence for cations is due to the stronger binding of remaining electrons.

The Cr $2p_{3/2}$ and Cr $2p_{1/2}$ spectra of Cr^{3+} phases commonly display multiplet splitting, which can be recognized on the occurrence of multiple inflection points, shoulders, and peaks (Figure B1b). Multiplet splitting arises when an ion has unpaired electrons such as Cr^{3+} with the electron configuration $3p^6$ $3d^3$ (Biesinger et al. 2004, 2011). A core electron vacancy produced by the photoionization effect can result in the coupling of unpaired electrons in the core and the outer shell. This coupling effect can create a number of final states which will be seen in the photoelectron spectrum. The Cr $2p_{3/2}$ envelope of chromite shows discrete multiplet structure (Fig. 2b) while spectra for Cr^{3+} hydroxides and Cr^{6+} compounds display either less resolved multiplet splitting or no multiplet splitting at all (Biesinger et al. 2004, 2011). The multiplet splitting in the Cr $2p_{3/2}$ envelope for an untreated surface of chromitite can be recognized on two peaks at 576 and 577 eV, an inflection point at 578 eV and a small shoulder at 579 eV (Figure B1b). As Cr^{3+} occurs predominantly in chromite, each of the bands fitted below the envelope corresponds to a structural component on the surface of the chromite grains.

Within the structure of chromite, $FeCr_2O_4$, Cr and Fe are completely ordered to the octahedral and tetrahedral positions, respectively, making it a '*normal'* spinel. As such, each O atom in the structure of chromite bonds to three [6]-coordinated cation (Cr) and one [4]-coordinated cation (Fe). Oxygen atoms on the surface of a solid bond to fewer cations than those in the bulk structure. Hence, there are six possible surface terminations for any given O atom: $^{[4]}Fe^{2+}$-O, $^{[6]}Cr^{3+}$-O, $^{[6]}$Cr-O-$^{[6]}$Cr, $^{[4]}$Fe-O-$^{[6]}$Cr, $^{[4]}Fe^{2+}$-O- 2x $^{[6]}Cr^{3+}$, and 3x $^{[6]}Cr^{3+}$-O (*i.e*. the surface termination $^{[4]}Fe^{2+}$-O-2x $^{[6]}Cr^{3+}$ contains one tetrahedrally coordinated Fe^{2+} and two octahedrally coordinated Cr^{3+} which bond to same surface O-atom).

In the spinel structure, each of the four bonds (1x $^{[4]}Fe^{2+}$-O and 3x $^{[6]}Cr^{3+}$-O) incident to the O atom has a bond strength of 0.5 vu (valence unit) totaling a sum of 2.0 vu, in accordance with Pauling's second rule which requires the sum of incident bond strengths to equal the formal charge of the anion (*i.e*., 2.0 vu in the case of O^{2-}). On the surface of chromite, the underbonded O atoms receive (formally) less than the required 2 *vu*; depending on whether the underbonded O atom is [3]-, [2]- or [1]-coordinated, the incident bond strength sums are either 1.5, 1.0 or 0.5 vu*,* respectively. Hence, a surface O atom is progressively less underbonded in terminations involving one (*e.g*. $^{[6]}Cr^{3+}$-O), two (*e.g*., $^{[6]}Cr^{3+}$-O-$^{[6]}Cr^{3+}$), and three cations ($^{[4]}Fe^{2+}$-O-2x$^{[6]}Cr^{3+}$). In the former types of terminations, the O atom forms a stronger covalent bond with the cations than in the latter type of surface terminations. An increase in covalency of a metal-oxygen (*M*-*O*) bond commonly results in a shift in electron density from O to *M* (*M* = $^{[4]}Fe^{2+}$, $^{[6]}Cr^{6+}$), which increases the electron density around *M* and thus decreases the binding energy of the photoelectrons (Schindler et al. 2009a, b). Hence, bands for surface terminations with a lower and higher number of *M* (*M* = $^{[4]}Fe^{2+}$, $^{[6]}Cr^{6+}$) occur at lower and higher binding energies, respectively. The same considerations can be done for protonated surface terminations. The covalency of the *M*-O bond decreases with the number of hydrogens bonding to O and thus bands corresponding to *M*-*O* bonds occur at lower binding energies than those for *M*-OH and *M*-OH_2 (Schindler et al. 2009a, b). Consequently, bands corresponding to surface terminations with bonds of low covalency such as $^{[4]}Fe^{2+}$-O-2x$^{[6]}$Cr or $^{[6]}Cr^{3+}$-OH-$^{[6]}Cr^{3+}$ most likely overlap at higher binding energies with each other and with bands corresponding to Cr^{6+}-O surface terminations.

Biesinger, M.C., Brown, C., Mycroft, J.R., Davidson, R.D. and McIntyre N.S. (2004) X-ray photoelectron spectroscopy studies of chromium compounds Surface and Interface Analysis **36**, 1550–1563

Biesinger, M.C., Paynec, B.B., Grosvenord, A.P., Laua, L.W.W., Gerson, A.R. and Smart R.S.C. (2011) Resolving surface chemical states in XPS analysis of first row transition metals, oxides and hydroxides: Cr, Mn, Fe, Co and Ni. Applied Surface Science 257, 2717–2730

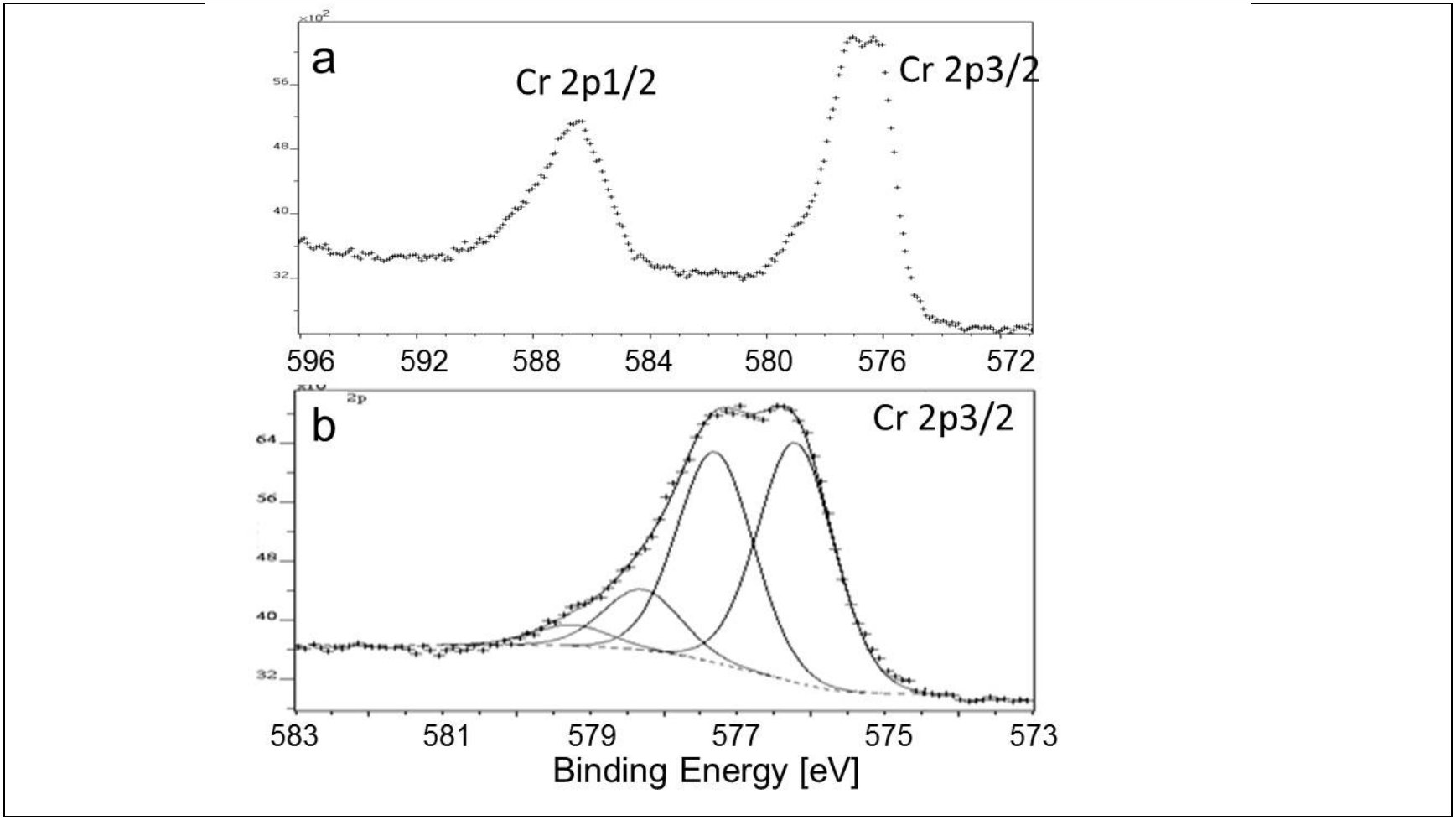

Figure B1 (a) the Cr 2p spectrum of an untreated chromitite surface depicting envelopes of the Cr $2p_{3/2}$ and Cr $2p_{1/2}$ photoelectrons; (b) the fitted envelope of the Cr $2p_{3/2}$ spectrum with bands assigned to peaks, inflection points and shoulders of the envelope; this type of multiplet splitting is characteristic for anhydrous Cr^{3+} compounds;